Radio-frequency-driven dipole-dipole interactions in spatially separated volumes

Tauschinsky, A.; van Ditzhuijzen, C.S.E.; Noordam, L.D.; van Linden van den Heuvell, H.B.

DOI
10.1103/PhysRevA.78.063409

Publication date
2008

Document Version
Final published version

Published in
Physical Review A

Radio-frequency-driven dipole-dipole interactions in spatially separated volumes

Atreju Tauschinsky, C. S. E. van Ditzhuijzen, L. D. Noordam, and H. B. van Linden van den Heuvell*
Van der Waals-Zeeman Institute, University of Amsterdam, Valckenierstraat 65, 1018 XE Amsterdam, The Netherlands
(Received 12 August 2008; published 5 December 2008)

Radio-frequency (rf) fields in the MHz range are used to induce resonant energy transfer between cold Rydberg atoms in spatially separated volumes. After laser preparation of the Rydberg atoms, dipole-dipole coupling excites the 49*s* atoms in one cylinder to the 49*p* state while the 41*d* atoms in the second cylinder are transferred down to the 42*p* state. The energy exchanged between the atoms in this process is 33 GHz. An external rf field brings this energy transfer into resonance. The strength of the interaction has been investigated as a function of amplitude (0–1 V/cm) and frequency (1–30 MHz) of the rf field and as a function of a static-field offset. Multiphoton transitions up to fifth order as well as selection rules prohibiting the process at certain fields have been observed. The width of the resonances has been reduced compared to earlier results by switching off external magnetic fields of the magneto-optical trap, making sub-MHz spectroscopy possible. All features are well reproduced by theoretical calculations taking the strong ac Stark shift due to the rf field into account.

DOI: 10.1103/PhysRevA.78.063409 PACS number(s): 32.80.Ee, 42.50.Hz, 32.80.Wr, 34.20.Cf

I. INTRODUCTION

Rydberg atoms have appealing properties for the study of atom-atom interactions; in particular, their lifetime is very long and their large (transition) dipole moments make them extremely sensitive to electric fields. Rydberg atoms can be used as sensitive probes of the environment or vice versa: the sensitivity to electric fields makes it easy to control their behavior through the application of external fields.

Resonant interactions between dipoles are of great interest in a broad range of fields and manipulating the coupling between dipoles is very useful in such diverse areas of physics as nanophotonics and quantum computation. Dipole-interacting Rydberg atoms are under active study by various groups as reported in Refs. [1–6], as an ideal system to investigate such interactions.

Previously [7] we investigated the dipole coupling between Rydberg atoms in two separated volumes as a function of static electric field, minimum particle distance, and interaction time. In the present paper we report how a radio-frequency field can provide additional control over the interaction strength. Radio-frequency and microwave fields have previously been used to investigate the properties of both isolated and interacting Rydberg atoms, e.g., in [2,8–11]. The techniques presented in this paper will allow precision spectroscopy on two-atom states and might be useful in quantum computation schemes to minimize electric-field inhomogeneities, which influence the dephasing of qubits implemented as Rydberg atoms [8].

In the experiment presented in this paper we create two spatially separated volumes of Rydberg atoms by exciting cold ground-state atoms from a magneto-optical trap. This is achieved by focusing two dye lasers tuned to different Rydberg states into the trap (see Fig. 1). This procedure creates a few tens of Rydberg atoms in each laser focus. After letting the atoms interact for a fixed period of time, they are field ionized, providing information on the states present. From this one can determine the number of atoms in the initial and final states, and hence the fraction of atoms having interacted. The interaction is influenced by external fields during the interaction time.

Figure 1 shows a schematic picture of the experiment. The photon associated with the dipole-dipole interaction is symbolized by the arrow between the two atoms. The other arrows represent external rf and static electric fields. During the interaction time the interaction is tuned into resonance by these externally applied fields. An additional external field due to blackbody radiation is always present in the experiment.

Figure 2 shows an illustration depicting the order of magnitude of the typical energy density of all time-dependent fields. Note that the energy density has been multiplied by ω giving units of J/m^3 as this leads to constant intervals $d\omega$ in the logarithmic plot. Also note that the scale of the y axis covers more than 20 orders of magnitude. This shows that

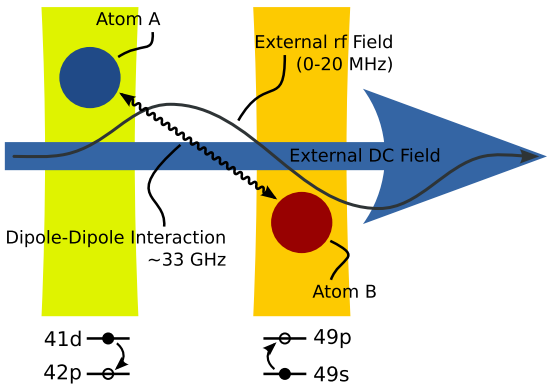

FIG. 1. (Color online) Schematic of the experiment. Fields are represented by the labeled arrows. The two upright areas symbolize the laser beams creating the Rydberg atoms. Only two atoms are shown for simplicity while in reality there are some tens of atoms in total. The Rydberg volumes are typically 25 μm apart at a width of 15 μm. The change of states of the Rydberg atoms is also depicted.

*H.B.vanLindenvandenHeuvell@uva.nl

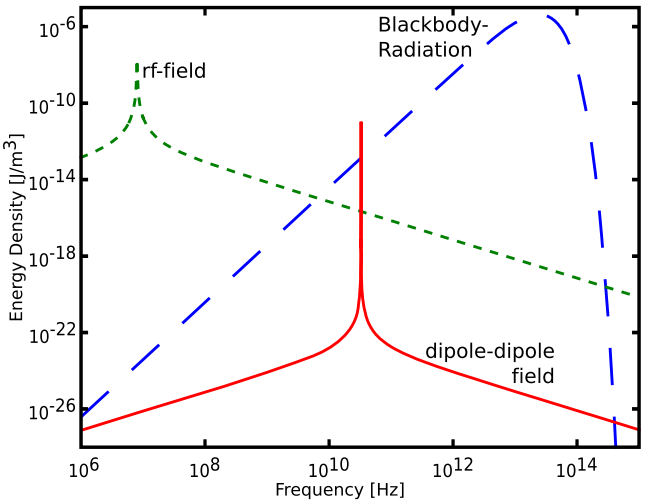

FIG. 2. (Color online) Energy density spectrum of the three different radiation fields, to which the atoms are exposed. The blue line (long dashes) represents the always and everywhere present blackbody radiation, depicted for 300 K. Resonances of the vacuum chamber and the metallic field plates are not taken into account for this illustration. The red line (solid) represents the photon that goes from one atom to the other, due to the dipole-dipole interaction at 25 μm. The line shape is Lorentzian based on experimental parameters. The green line (dashed) represents the oscillating field that is externally applied.

while there is a contribution of the blackbody radiation in the background, the contribution of the dipole-dipole and rf fields is much larger in the relevant frequency ranges.

The process in our experiment can be interpreted as amplitude modulation of the dipole field by the external rf field. Surprisingly, the amplitude of the carrier wave (dipole-dipole radiation) is much smaller than the amplitude of the modulating rf field.

II. RADIO-FREQUENCY-ASSISTED DIPOLE-DIPOLE INTERACTIONS

The initial states chosen in this experiment are $41d$ and $49s$, created in separate volumes. They exchange a photon in a resonant dipole-dipole interaction forming the states $42p$ and $49p$ in one of the processes

$$41d_{3/2,1/2} + 49s_{1/2,1/2} \rightarrow 42p_{1/2,1/2} + 49p_{3/2,1/2}, \quad (1a)$$

$$41d_{3/2,1/2} + 49s_{1/2,1/2} \rightarrow 42p_{1/2,1/2} + 49p_{3/2,3/2}, \quad (1b)$$

where the notation denotes $n\ell_{j,|m_j|}$. Both the $41d_{3/2}$ and the $49p_{3/2}$ states split in an electric field into two substates $|m_j| = 1/2$ and $|m_j| = 3/2$. Note that the initial $41d_{3/2,3/2}$ state is not excited by the laser, because of its polarization, so it does not play a role in our experiment and was ignored in Eq. (1). The approach of using four different states makes it possible to control the distance between the atoms, by having separate volumes for the two different initial states. A position-resolved detection technique is then not necessary; state-selective detection of the final $49p$ state will probe the dipole-dipole interaction.

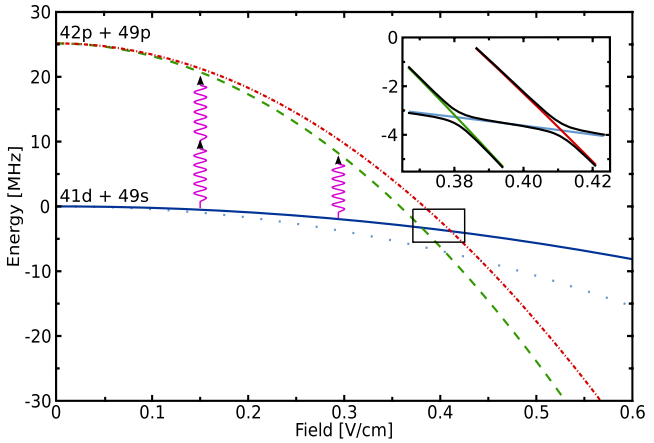

FIG. 3. (Color online) Schematic representation of two-atom energy versus electric field. An external rf field of 10 MHz is symbolized by the arrows. At a purely static field of 0.38 V/cm and 0.41 V/cm the dipole-dipole transition is resonant. At 0.3 V/cm it is brought into resonance by one rf photon of 10 MHz, while at 0.15 V/cm two such photons bring the system into resonance. The inset shows the avoided crossings due to dipole-dipole interaction at a separation of 25 μm.

The binding energies and polarizabilities of the states from Eqs. (1) are obtained from a calculated Stark map, using the Numerov method [12] and making use of the rubidium-85 quantum defects given in [13–15]. In Fig. 3 the sum of the binding energies of the two atoms is plotted versus the electric field. Both the initial state ($41d+49s$) as well as the final state ($42p+49p$) undergo a purely quadratic Stark shift, which is much stronger for the final pp state than for the initial sd state. This is caused by the strong Stark shift of the $49p$ state.

For the dipole-dipole transfer to become resonant the energy difference between the initial and final two-atom state has to be zero. This energy difference can be written as

$$W = W_0 - \frac{1}{2}\alpha F^2, \quad (2)$$

where W_0 is the zero-field energy difference, $W_0 = 25.15(13)$ MHz, F is the total electric field, and α is the difference polarizability, i.e., the difference in polarizability between the initial and the final two-atom state. The nonlinear term in the field is due to the purely quadratic Stark shift of the energy levels. The energy difference at zero field (W_0) is already very small, which is one of the reasons we have chosen this particular process. The difference polarizabilities are $\alpha_a = 347.04(4)$ MHz/(V/cm)^2 for process (1a) and $\alpha_b = 297.40(4)$ MHz/(V/cm)^2 for process (1b); this makes the process resonant at the static fields $F_a = 0.3807(15)$ V/cm and $F_b = 0.4113(16)$ V/cm, respectively.

For nonzero electric fields the quantum number ℓ does not describe a proper eigenstate of the system. We label those states as having the angular momentum quantum number ℓ that connect adiabatically to the zero-field states with that quantum number. However, at an electric field of 0.4 V/cm the mixing in of other ℓ states is still negligible.

The strength of the dipole-dipole interaction, and therefore half the size of the avoided crossing is given in atomic units by

$$V = \frac{\boldsymbol{\mu_1}\cdot\boldsymbol{\mu_2} - 3(\boldsymbol{\mu_1}\cdot\hat{\mathbf{R}})(\boldsymbol{\mu_2}\cdot\hat{\mathbf{R}})}{R^3}, \tag{3}$$

where $\mathbf{R}$ is the distance vector between the interacting particles, $\boldsymbol{\mu_1}$ is the dipole moment of the $41d \rightarrow 42p$ transition, and $\boldsymbol{\mu_2}$ is the dipole moment of the $49s \rightarrow 49p$ transition. The dipole moments are rather large, of the order of $1000a_0e$, which is another advantage of this particular process equation (1). The exact value and polarization of each dipole μ depends on the Δm_j of the transition. The dipole is either linearly polarized ($\boldsymbol{\mu}=\mu_z$) or circularly polarized ($\boldsymbol{\mu}=\mu_x \pm i\mu_y$). For the field strength of the oscillating dipoles we typically obtain 34 μV/cm at a separation of 25 μm. We can consider the dipole-dipole interaction process as the exchange of a photon from one atom to the other. This photon has an energy of 32.8 GHz. The inset in Fig. 3 shows the avoided crossing due to the dipole-dipole interaction for this separation. The frequency of the quantum beat oscillation of the system (or the Rabi oscillation of the single atoms) is $\omega_{QB}=2V\approx 2\pi\times 200$ kHz.

In the presence of an external rf field the *sd* state can couple to the *pp* state even far away from the static-field resonance, as symbolized by the arrows in Fig. 3. This is the case if the energy of the rf photon equals the energy difference between the *sd* and *pp* state. The energy difference of those states for an rf field is

$$W = W_0 - \frac{1}{2}\alpha(F_S + F_{\mathrm{rf}}\sin\omega t)^2, \tag{4}$$

where F_S is the static-field offset and F_{rf} is the amplitude of the radio-frequency field. As long as $\omega_{QB} \ll \omega$ we can average Eq. (4) over time [2]; this yields

$$W = W_0 - \frac{1}{2}\alpha\left(F_S^2 + \frac{1}{2}F_{\mathrm{rf}}^2\right), \tag{5}$$

and we define an effective field

$$F_{\mathrm{eff}} = \sqrt{F_S^2 + \frac{1}{2}F_{\mathrm{rf}}^2}. \tag{6}$$

This effective field is defined such that the Stark shift for a static field equal to F_{eff} is the same as the time-averaged Stark shift of the time-dependent field. The rf field brings the dipole-dipole interaction into resonance, if an integer number of rf photons matches the energy difference W between the states, so

$$N\omega = W_0 - \frac{1}{2}\alpha F_{\mathrm{eff}}^2, \tag{7}$$

where N is the number of photons involved in the transition and ω is the frequency of the external rf photon. Note that in the case of a purely linear Stark shift the behavior is essentially different. In that case the time average of the rf field becomes zero and only the static field F_S is relevant. The term $\frac{1}{4}\alpha F_{\mathrm{rf}}^2$ in Eq. (5) is also called the ac Stark shift.

III. IMPROVED EXPERIMENTAL SETUP

In this experiment a similar setup to measure dipole-dipole transitions is used as in earlier experiments described in [7,16]. A magneto-optical trap (MOT) is used to create a cold cloud of ^{85}Rb atoms. Rubidium atoms from a dispenser 3 cm away are trapped and cooled by three orthogonal pairs of counterpropagating laser beams in a quadrupole magnetic field. The cold atom cloud contains typically several 10^7 atoms at a temperature well below 300 μK. Charged particles emitted by the dispenser are deflected by statically charged plates in front of the dispenser. The background pressure is below 3×10^{-8} mbar. These conditions ensure that the atoms in the MOT do not move on the relevant time scales of the experiment.

Rydberg atoms are created by 8 ns laser pulses at 594 nm in a two-photon process from the cold ground-state Rb atoms. There are two separate sets of Nd:YAG-pumped dye lasers: one which excites atoms to the 49*s* state and one which excites atoms to the 41*d* state. The laser creating the 49*s* atoms has a linewidth of 0.017(11) cm^{-1} and a pulse energy of 3.0(1) μJ; the laser creating 41*d* atoms has a linewidth of 0.21(2) cm^{-1} and a pulse energy of 5.0(1) μJ. The repetition rate of both lasers is 10 Hz. Each can be focused into a different region of the MOT to create two spatially separated, cigar-shaped volumes of Rydberg atoms within the magneto-optical trap. The focus of the laser creating the 49*s* atoms can be moved laterally within the trap by the use of a stepper motor. The beam separation can accurately be measured in a two-photon mixing process using one photon from each beam. For this measurement we detune the laser creating the 49*s* atoms by 20 GHz to the blue and make sure that the laser pulses overlap in time. This leads to the excitation of the 44*d* state as described in [7]. As reported there the diameter of the Rydberg volumes is 11.6(0.4) μm for 49*s* atoms and 16.3(0.5) μm for 41*d* atoms.

The MOT is situated between two circular stainless-steel plates with a diameter of 5.5 cm, which are spaced 2.50(5) cm apart. Both plates are perforated by a 14-mm hole in the center to allow ionization products to pass through, as well as to enable optical access to the MOT. These plates serve to generate the static and radio-frequency fields used to manipulate the dipole-dipole interaction as well as for the field ionization.

The manipulating fields are generated by an Agilent 33250A arbitrary waveform generator attached to one of the plates. The amplitude of these external fields is in the range of 0–1 V/cm and the frequency of the external rf field is in the range of 1–30 MHz. The polarization of the rf field is always parallel to the separation between the Rydberg volumes as they are separated along the symmetry axis of the plates.

The other plate is connected to a home-built fast high-voltage pulse generator to provide a negative-field ramp that ionizes the Rydberg atoms after the interaction time. The ramp rises from 0 to 150 V/cm in 5 μs. Electrons are detected on a Hamamatsu multichannel plate (MCP). Since each state ionizes at a different electric field the signal arises at a different time for different states [17]. This allows one to distinguish between 49*s*, 49*p*, and 41*d* atoms. Electrons from

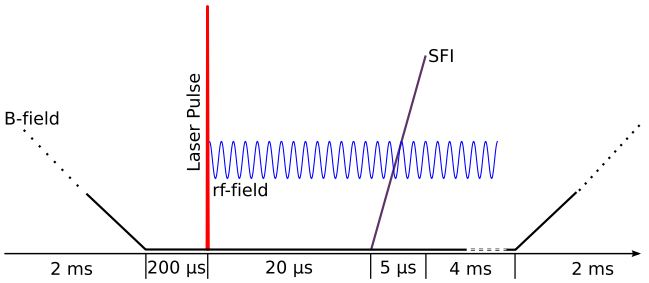

FIG. 4. (Color online) Schematic of the timing of one experimental cycle. First, the magnetic field is switched off, a laser pulse excites Rydberg states, which then are field ionized after 20-μs interaction time. Finally, the magnetic field is switched on again.

41d atoms arrive at the same time as electrons from 42p, so this method does not allow a distinction between these two states. We use the final state fraction $N_{49p}/(N_{49p}+N_{49s})$ as a measure of the dipole-dipole interaction.

It is important that both power supplies connected to the plates have a low noise level during the interaction time. This was realized by a metal shielding box around the home-built pulse generator and an implemented line filter. The Agilent 33250A had a low noise level already. The total level of electric-field noise is below 2 mV/cm. We did not observe any influence of the rf field on the selective field ionization (SFI) process as the amplitude of the rf field is negligible compared with the magnitude of the SFI pulse, and as the frequency of the rf field is too low to induce transitions to neighboring Rydberg states.

We have greatly improved our setup by adding the ability to switch the coils generating the magnetic quadrupole field for the MOT off during the dipole-dipole interaction time. Previously the magnetic field varied by ≈0.5 G over the length of the Rydberg volumes. This resulted in a broadening of the resonances by ≈1.5 MHz, due to Zeeman shifts of the involved states. For all results reported here the coils were switched off for 6 ms in each 100-ms cycle using a fast home-built insulated gate bipolar transistor switch. The current in the coils decays with a decay time of 25 μs. Measurements are performed 2.2 ms after the coils were switched. The magnetic field has been measured to be below 0.14 G at this time. The remaining field is assumed to be due to background stray fields. The timing sequence of the experiment is shown in Fig. 4.

Figure 5 shows the 49p fraction $N_{49p}/(N_{49p}+N_{49s})$ as a function of static electric field for various separations of the dye laser beams creating the Rydberg atoms. The widths of the resonances have been improved significantly compared to the results presented in [7] and are given in Table I. Resonance widths are extracted from the data by fitting two independent Lorentz profiles to the measurements. The improvement is clearly due to the switching of the magnetic field. Our results are now in good agreement with the results of simulations [7], which are also given in Table I. The remaining difference might be due to remaining variations in the electric field, or due to ions in the MOT cloud. Note that a width of 5 mV/cm corresponds to only 661 kHz for resonance F_a and 612 kHz for resonance F_b. Both the simulations as well as the measurements yield widths bigger than

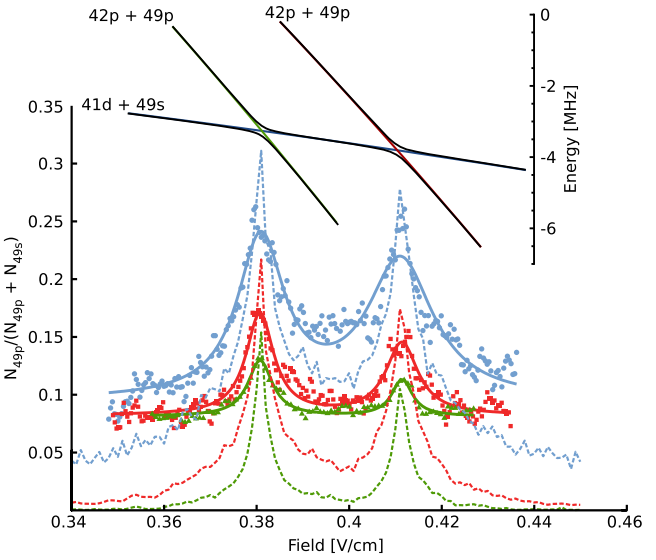

FIG. 5. (Color online) Static-field scans at 20- (blue circles), 30- (red squares), and 40- (green triangles) μm separation between the 41d and the 49s volumes. Solid lines are fits with two independent Lorentz profiles. Dashed lines are theoretical computations [7]. The inset shows the energy-level diagram for two atoms at 25 μm. The energy scale is relative to the energy of the 41d+49s state at zero field.

the theoretical predictions of 200 kHz. This discrepancy can be attributed to many-body effects as well as the finite width of the Rydberg volumes. Both effects are taken into account in the simulations. In all further measurements discussed in this paper a beam separation of 25 μm is used.

IV. DIABATIC SWITCHING OF THE DIPOLE-DIPOLE INTERACTION

In a first experiment we investigated the switching of the dipole-dipole interaction by repeatedly changing the electric field diabatically from the resonance F_a to a value $F_{\text{off}}=0$ V/cm. The results are shown in Fig. 6. This figure depicts the 49p fraction as a function of interaction time. The main curve in Fig. 6 (red solid lines, triangles) shows the 49p fraction for an electric field that is switched several times from 0 V/cm to F_a and back again. The switching is done at a very fast rate of 76 V/(cm μs). This is much faster than the frequency of the quantum beat oscillations times the width of the resonance [2×10^{-4} V/(cm μs)] ensuring that the system

TABLE I. Width (FWHM) of the resonances F_a and F_b for varying beam separations. Experimental and theoretical values are given. Theoretical data is taken from [7].

	FWHM (F_a) mV/cm		FWHM (F_b) mV/cm	
	Experiment	Theory	Experiment	Theory
20 μm	12.3(1.3)	11.0(1.3)	17.3(1.9)	11.5(1.5)
30 μm	7.3(0.8)	8.1(0.9)	8.5(1.3)	7.8(1.0)
40 μm	6.4(0.9)	4.2(0.3)	5.3(1.2)	4.4(0.5)

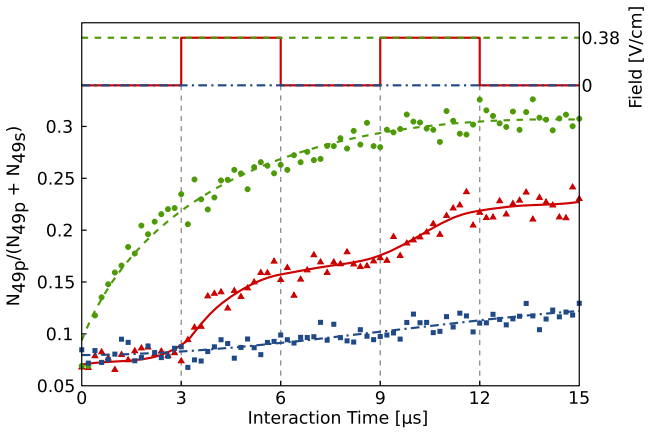

FIG. 6. (Color online) 49p fraction as a function of interaction time for different fields $F=F_a$ (green circles), $F=0$ (blue squares), and F alternating between F_a and 0 in the manner depicted on top of the figure (red triangles). Lines depict a smooth spline fitted to the data.

follows the field diabatically. Clearly the 49p fraction rises during the times where $F=F_a$ and stagnates when $F=F_{\text{off}}$. This shows how the dipole-dipole interaction can be switched on and off by rapidly changing the electric field. Reference measurements are performed for $F=F_a$ at all times (green dashed curves, circles) and for $F=0$ at all times (blue dashed-dotted curves, squares). In the first case the 49p fraction rises in the manner already measured in [7]. When the field is off resonant at all times there is a small background contribution due to blackbody radiation (see Fig. 2).

V. OBSERVATION OF rf-ASSISTED MULTIPHOTON DIPOLE-DIPOLE TRANSITIONS

Figure 7 shows the 49p fraction as a function of the frequency of an external sinusoidal rf field with constant amplitude and offset. Here $F_S=260$ mV/cm and $F_{\text{rf}}=80$ mV/cm. In this case amplitude and offset are chosen such that the field never reaches the resonance fields F_a or F_b. The figure shows a series of double peaks; each subpeak corresponds to one of the two resonances from the different $|m_j|$ substates, and each set corresponds to a different number of photons (N) needed to make the transition resonant, as noted in the figure. Up to five photon transitions are clearly visible in the figure. The frequency of each N-photon transition is $1/N$th of the one-photon transition frequency. The position of the peaks agrees very well with theoretical calculations based on Eq. (7) indicated by vertical lines (dashed, F_a; dotted, F_b) calculated for an effective field of $F_{\text{eff}}=266.1$ mV/cm.

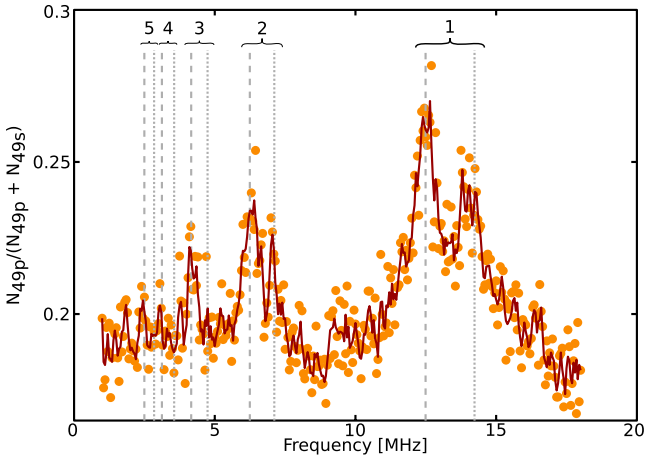

FIG. 7. (Color online) Observed frequency dependence of rf-assisted dipole-dipole transitions at $F_S=0.26$ V/cm. Multiphoton peaks with $n=1-5$ involved photons are clearly distinguishable; the number of involved photons is denoted in the figure. The double peak structure corresponds to the two resonances F_a and F_b. The solid line is a smooth spline fitted to the data.

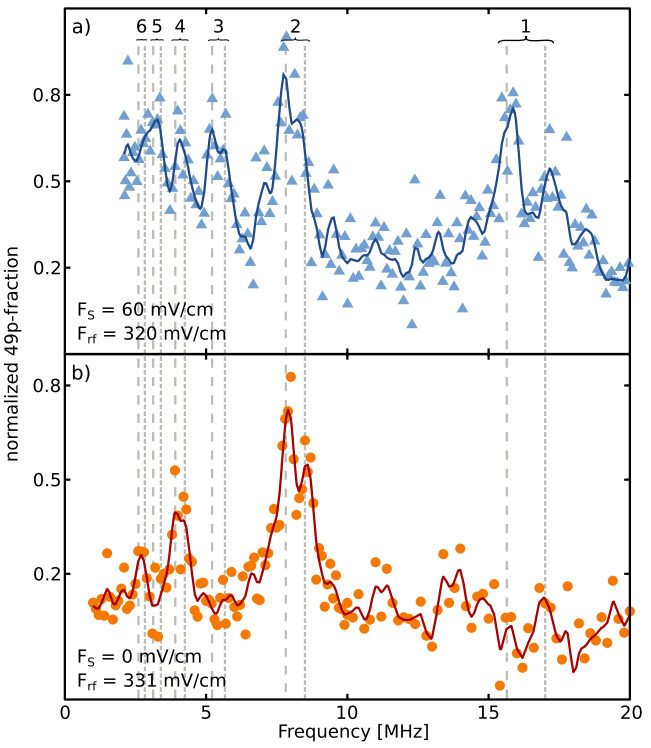

FIG. 8. (Color online) Measurements at small static field F_S (upper panel) and at $F_S=0$ (lower panel) showing selection rules prohibiting odd photon number transitions (see the text). The solid lines are a smooth spline fitted to the data.

Figure 8 again shows the 49p fraction (normalized to the highest measured signal) as a function of frequency of the rf field. The lower panel shows a frequency scan for $F_S=0$ V/cm and $F_{\text{rf}}=331$ mV/cm, hence no static field is present in this measurement. The upper panel uses a small static field of $F_S=60$ mV/cm and $F_{\text{rf}}=320$ mV/cm so both measurements have the same effective field $F_{\text{eff}}=234$ mV/cm. All peaks with an odd photon number are clearly suppressed in the lower panel, but easily distinguishable in the upper panel. This can be understood on the basis of selection rules: The dipole-dipole interaction Eq. (1) requires that one unit of angular momentum is transferred from one atom to the other, $49s \rightarrow 49p$ requires $\Delta\ell=+1$ and $41d \rightarrow 42p$ requires $\Delta\ell=-1$. To achieve this, an odd number of photons must be involved in the process. Since there is already one photon transmitting the dipole-dipole interaction the number of external rf photons must be even if the static

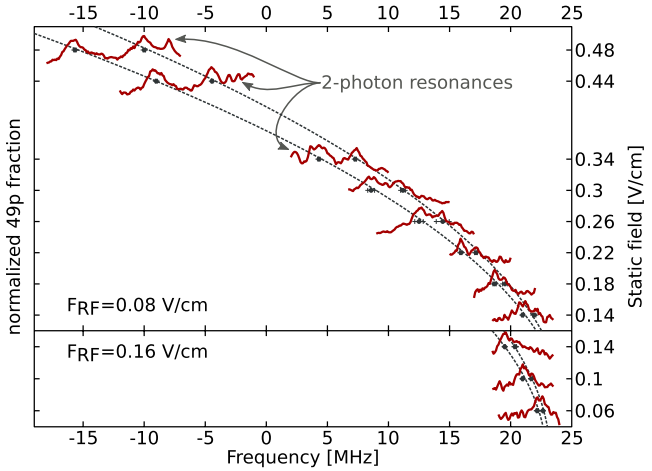

FIG. 9. (Color online) +1 and −1 photon resonances at various effective field values. In the lower panel (small static fields) the rf amplitude had to be increased leading to a larger ac Stark shift. The fitted resonance positions are marked by black dots. Some two-photon resonances are also visible and marked in the figure.

field is zero. Already at static fields of only 60 mV/cm this selection rule becomes invalid as a static-field photon can account for the missing angular momentum without transferring any energy.

In Fig. 8 the importance of the ac Stark shift can clearly be observed. For example, for resonance *a*, the energy difference between the *sd* and the *pp* state is 24.53 MHz at 60 mV/cm. Without ac Stark shift the one-, two-, and three-photon resonances are expected at 24.53, 12.26, and 8.17 MHz. Including the ac Stark shift

$$\Delta\omega = \frac{1}{4}\alpha F_{\mathrm{rf}}^2, \tag{8}$$

we get significantly different numbers, i.e., 15.64, 7.82, and 5.31 MHz. These resonant positions clearly correspond to the observed peaks. The theoretical predictions including this ac Stark shift are depicted in the figure as dash-dotted lines (resonance *a*) and dotted lines (resonance *b*).

In Fig. 9 the one-photon resonance is used to perform spectroscopy on the two-atom states, measuring the energy difference between initial and final states for several values of static-field offset. The figure shows the 49*p* fraction as a function of both rf and static field. The position of the peaks corresponds to the energy levels in Fig. 3 as depicted by the dashed lines. These dashed lines are the same as the difference between the energy levels depicted in Fig. 3, but now with the *x* and *y* axis interchanged. In the upper panel the amplitude of the radio-frequency field is F_{rf}=80 mV/cm. In the lower panel F_{rf}=160 mV/cm was used since the signal dropped too much for the lower amplitude at these small static-field values. This leads to an appreciable contribution of the ac Stark shift in the lower panel. The dashed lines show the theoretical resonance position taking ac Stark shift into account on the basis of Eq. (7). The +1 and −1 photon resonance position as a function of the static field allows us to determine the total difference polarizability and difference energy between the initial and final state. For the states investigated in this paper this yields W_0=25.07(10) MHz, α_a=347.2(2.1) MHz/(V/cm)^2 and α_b=300.5(1.9) MHz/(V/cm)^2. Note that for these results the field strength was calibrated using static-field scans such as shown in Fig. 5. For accurate spectroscopy independent measurements of the electric-field strength would be needed.

VI. CONCLUSION

The results presented in this paper have been improved significantly compared to [7] by switching off the magnetic-field coils during measurements. The widths of the resonance peaks are now in good agreement with the simulations presented in [7]. This improvement makes sub-MHz spectroscopy possible. We have shown that the dipole-dipole interaction can be manipulated by rapidly switching the electric field. Furthermore, we have shown multiphoton resonances in a rf-assisted dipole-dipole interaction with up to five involved photons where the interacting dipoles are localized in separate volumes. For large amplitudes of the rf field significant ac Stark shifts can be observed due to the quadratic field dependence of the involved states. The positions of the resonance peaks agree well with the theory presented here. The methods explored in this paper allow one to perform spectroscopy on Stark states of two Rydberg atoms and we have determined the energy difference and difference in polarizability with good precision.

In this paper we have shown several versatile methods of manipulating the interactions between Rydberg atoms in separated volumes by external fields. These methods should prove to be valuable for the manipulation of dipole-dipole interaction between neutral atoms.

ACKNOWLEDGMENTS

We thank Richard Newell for contributions to the experiment and Francis Robicheaux for stimulating discussions. This work is part of the research program of the Stichting voor Fundamenteel Onderzoek der Materie (FOM), which is financially supported by the Nederlandse Organisatie voor Wetenschappelijk Onderzoek (NWO).

[1] K. Afrousheh, P. Bohlouli-Zanjani, D. Vagale, A. Mugford, M. Fedorov, and J. D. D. Martin, Phys. Rev. Lett. **93**, 233001 (2004).

[2] Y. Zhang, M. Ciocca, L.-W. He, C. E. Burkhardt, and J. J. Leventhal, Phys. Rev. A **50**, 1101 (1994).

[3] W. Li, P. J. Tanner, and T. F. Gallagher, Phys. Rev. Lett. **94**, 173001 (2005).

[4] T. Vogt, M. Viteau, J. Zhao, A. Chotia, D. Comparat, and P.

Pillet, Phys. Rev. Lett. **97**, 083003 (2006).
[5] S. Westermann, T. Amthor, A. L. de Oliveira, J. Deiglmayr, M. Reetz-Lamour, and M. Weidemüller, Eur. Phys. J. D **40**, 37 (2006).
[6] T. A. Johnson, E. Urban, T. Henage, L. Isenhower, D. D. Yavuz, T. G. Walker, and M. Saffman, Phys. Rev. Lett. **100**, 113003 (2008).
[7] C. S. E. van Ditzhuijzen, A. F. Koenderink, J. V. Hernandez, F. Robicheaux, L. D. Noordam, and H. B. van Linden van den Heuvell, Phys. Rev. Lett. **100**, 243201 (2008).
[8] P. Bohlouli-Zanjani, J. A. Petrus, and J. D. D. Martin, Phys. Rev. Lett. **98**, 203005 (2007).
[9] T. F. Gallagher, K. A. Safinya, F. Gounand, J. F. Delpech, W. Sandner, and R. Kachru, Phys. Rev. A **25**, 1905 (1982).
[10] L. A. Bloomfield, R. C. Stoneman, and T. F. Gallagher, Phys. Rev. Lett. **57**, 2512 (1986).
[11] P. Pillet, R. Kachru, N. H. Tran, W. W. Smith, and T. F. Gallagher, Phys. Rev. A **36**, 1132 (1987).
[12] M. L. Zimmerman, M. G. Littman, M. M. Kash, and D. Kleppner, Phys. Rev. A **20**, 2251 (1979).
[13] W. Li, I. Mourachko, M. W. Noel, and T. F. Gallagher, Phys. Rev. A **67**, 052502 (2003).
[14] J. Han, Y. Jamil, D. V. L. Norum, P. J. Tanner, and T. F. Gallagher, Phys. Rev. A **74**, 054502 (2006).
[15] K. Afrousheh, P. Bohlouli-Zanjani, J. A. Petrus, and J. D. D. Martin, Phys. Rev. A **74**, 062712 (2006).
[16] C. S. E. van Ditzhuijzen, A. F. Koenderink, L. D. Noordam, and H. B. van Linden van den Heuvell, Eur. Phys. J. D **40**, 13 (2006).
[17] T. F. Gallagher, *Rydberg Atoms* (Cambridge University Press, Cambridge, England, 1994).